Autophagy enforces functional integrity of regulatory T cells by coupling environmental cues and metabolic homeostasis

Published in final edited form as:

Nat Immunol. 2016 March ; 17(3): 277–285. doi:10.1038/ni.3365.

Autophagy enforces functional integrity of regulatory T cells by coupling environmental cues and metabolic homeostasis

Jun Wei[1], **Lingyun Long**[1], **Kai Yang**[1], **Cliff Guy**[1], **Sharad Shrestha**[1], **Zuojia Chen**[2], **Chuan Wu**[2], **Peter Vogel**[3], **Geoffrey Neale**[4], **Douglas R Green**[1], and **Hongbo Chi**[1]

[1]Departments of Immunology, St. Jude Children's Research Hospital, Memphis, Tennessee 38105, USA

[2]Evergrande Center for Immunologic Diseases, Brigham and Women's Hospital, Harvard Medical School, Boston, Massachusetts 02115, USA

[3]Department of Pathology St. Jude Children's Research Hospital, Memphis, Tennessee 38105, USA

[4]Hartwell Center for Bioinformatics and Biotechnology, St. Jude Children's Research Hospital, Memphis, Tennessee 38105, USA

Abstract

Regulatory T (T_{reg}) cells respond to immune and inflammatory signals to mediate immunosuppression, but how functional integrity of T_{reg} cells is maintained under activating environments remains elusive. Here we found that autophagy was active in T_{reg} cells and supported their lineage stability and survival fitness. T_{reg} cell-specific deletion of the essential autophagy gene *Atg7* or *Atg5* led to loss of T_{reg} cells, increased tumor resistance, and development of inflammatory disorders. Atg7-deficient T_{reg} cells had increased apoptosis and readily lost Foxp3 expression, especially after activation. Mechanistically, autophagy deficiency upregulated mTORC1 and c-Myc function and glycolytic metabolism that contributed to defective T_{reg} function. Therefore, autophagy couples environmental signals and metabolic homeostasis to protect lineage and survival integrity of T_{reg} cells in activating contexts.

Correspondence should be addressed to H.C. (; Email: hongbo.chi@stjude.org)

Accession codes

Gene Expression Omnibus: microarray data have been deposited under the accession code GSE75218.

Author contributions

J.W. designed and performed cellular, molecular, and biochemical experiments and wrote the manuscript; L.L. performed immunoblot analysis; K.Y. performed Seahorse assays and helped early development of the project; C.G. performed imaging assays; S.S., Z.C. and C.W. performed the TSDR methylation analysis; P.V. performed histopathology analysis; G.N. performed bioinformatic analysis; D.R.G. contributed genetic models; and H.C. designed experiments, wrote the manuscript, and provided overall direction.

Competing financial interests

The authors declare no competing financial interests.

Introduction

Regulatory T (T_{reg}) cells play an indispensable role in preventing autoimmune disease and establishing self-tolerance[1]. The activation states and functional capacities of T_{reg} cells are dynamically programmed by environmental signals[2]. T_{reg} cells emerge from the thymus as quiescent central T_{reg} cells (cT_{reg}; CD44^{lo}CD62L^{hi})[3]. In response to environmental cues in the periphery, a fraction of T_{reg} cells are continuously activated and converted into effector T_{reg} cells (eT_{reg}; CD44^{hi}CD62L^{lo}) under steady state[3,4]. After an inflammatory challenge, T_{reg} cells are further activated and potently upregulate their suppressive activity and contribute to the regulation of inflammatory responses induced by autoimmunity, tumor and other stimuli[5]. Thus, the activation states and functional capacities of T_{reg} cells are dynamically programmed by environmental signals. As for cell-intrinsic pathways, continued expression of Foxp3 is required to reinforce T_{reg} cell functional integrity[1]. While Foxp3 expression is stable *in vivo*[6], T_{reg} cells can lose Foxp3 expression and acquire effector function in certain inflammatory conditions[7–10], suggesting that activating environments could destabilize Foxp3 expression. Aside from lineage stability, maintenance of the anti-apoptotic program also contributes to the functional integrity of T_{reg} cells in maintaining immune tolerance[11].

Macroautophagy (herein referred to as autophagy) is an evolutionarily conserved self-digestive process that targets intracellular substrates for lysosomal degradation and recycling in response to stress and other environmental signals[12–14]. Autophagy plays important and context-dependent roles in T cell-mediated immune responses. For example, autophagy is required for survival and TCR-induced proliferation of T cells[15]. In contrast, activated CD8$^+$ cells deficient in autophagy exhibit normal proliferation and effector function, but with impaired memory cell formation[16]. Autophagy is induced after TCR and cytokine stimulation[15,17,18], but virus-specific CD8$^+$ T cells downregulate autophagy activity during clonal expansion, followed by induction of autophagy when they stop dividing[16]. These studies highlight dynamic and signal-dependent function and regulation of autophagy.

We report here that autophagy is actively regulated in T_{reg} cells, and serves as a central signal-dependent controller of T_{reg} cells by restraining excessive apoptotic and metabolic activities. We found that T_{reg} cell-specific loss of the essential autophagy gene *Atg7* or *Atg5* was sufficient to break self-tolerance while facilitating tumor clearance. Atg7-deficient T_{reg} cells exhibited impaired lineage stability and increased apoptosis, thereby compromising their functional integrity. Although autophagy is known to promote energy balance[14,17,19], we found that T_{reg} cells deficient in autophagy showed increased mTORC1 activity, c-Myc expression and glycolytic metabolism, characteristic of anabolic upregulation[20]. Inhibition of mTORC1 or c-Myc in Atg7-deficient T_{reg} cells partly restored T_{reg} cell stability and metabolic homeostasis. Collectively, our studies establish a crucial role of autophagy in establishing T_{reg} cell-mediated immune tolerance by coordinating immune signals and metabolic homeostasis to protect the functional integrity of T_{reg} cells.

RESULTS

Autophagy is functionally active in T_{reg} cells

To investigate regulation of autophagy in T_{reg} cells, we quantified autophagosomes in peripheral T_{reg} cells and naïve $CD4^+$ cells using transgenic mice expressing the green fluorescent protein (GFP) fused to LC3 (GFP-LC3), which labels autophagic membranes[21]. T_{reg} cells had significantly more cells labeled with GFP-$LC3^+$ puncta than did naïve $CD4^+$ cells (Fig. 1a), suggesting increased autophagosomes in T_{reg} cells. Lipidated LC3 (LC3-II) is another marker of autophagic membranes[12–14]; immunoblot analysis showed that T_{reg} cells had higher amount of LC3-II than naïve $CD4^+$ cells (Supplementary Fig. 1a). Treatment of cells with a lysosome inhibitor bafilomycin A1 (Baf1A), which blocks lysosome-mediated degradation of autophagosomes, increased the amount of LC3-II in both T_{reg} cells and naïve $CD4^+$ cells, but T_{reg} cells still had higher amount of LC3-II than naïve $CD4^+$ cells (Supplementary Fig. 1a). Therefore, T_{reg} cells have higher autophagy activity than naïve $CD4^+$ cells, indicating a possible role of autophagy in T_{reg} cells.

To test this hypothesis, we crossed mice with *lox*P-flanked *Atg7* alleles ($Atg7^{fl/fl}$) with $Foxp3^{YFP\text{-}Cre}$ ($Foxp3^{Cre}$) mice to delete the essential autophagy gene *Atg7* in T_{reg} cells (hereafter $Foxp3^{Cre}Atg7^{fl/fl}$). Deletion of *Atg7* abrogated autophagy in T_{reg} cells, as indicated by the absence of LC3-II in immunoblot analysis (Supplementary Fig. 1a). To determine whether T_{reg} cells require autophagy to suppress antitumor immune responses, we inoculated $Foxp3^{Cre}Atg7^{fl/fl}$ mice with MC38 colon adenocarcinoma cells. Tumor growth was severely inhibited in $Foxp3^{Cre}Atg7^{fl/fl}$ mice, suggesting that Atg7-deficient T_{reg} cells failed to inhibit antitumor immune response (Fig. 1b). Consistent with this notion, $Foxp3^{Cre}Atg7^{fl/fl}$ mice had greatly increased percentage of tumor-infiltrating $CD8^+$ cells (Supplementary Fig. 1b), and expression of interferon-γ (IFN-γ) in effector $CD4^+$ and $CD8^+$ T cells (Fig. 1c). However, $Foxp3^{Cre}Atg7^{fl/fl}$ mice had a profound loss of T_{reg} cells in the tumor site (Fig. 1d). These results identify a crucial role of Atg7 in endowing T_{reg} cells the ability to suppress antitumor immune responses.

T_{reg} deletion of Atg7 or Atg5 alters immune homeostasis

The indispensable role of Atg7 in maintaining T_{reg} cells in a pathological condition prompted us to determine the requirement of autophagy in T_{reg} cells in maintaining self-tolerance under homeostatic conditions. $Foxp3^{Cre}Atg7^{fl/fl}$ mice at 10–12 weeks of age developed lymphoid hyperplasia with increased cellularity of the spleen and peripheral lymph nodes (PLNs) (Fig. 1e, Supplementary Fig. 1c). $Foxp3^{Cre}Atg7^{fl/fl}$ mice contained a higher proportion of the effector or memory population ($CD44^{hi}CD62L^{lo}$) in the $CD4^+$ and $CD8^+$ compartments (Fig. 1f). Moreover, $CD44^{hi}$ cells from $Foxp3^{Cre}Atg7^{fl/fl}$ mice showed increased expression of IFN-γ and interleukin 17 (IL-17) (Fig. 1g), but not IL-4 (Supplementary Fig. 1d). Therefore, T cells from $Foxp3^{Cre}Atg7^{fl/fl}$ mice were spontaneously activated *in vivo*. Moreover, severe systemic inflammatory disorders were observed in aged $Foxp3^{Cre}Atg7^{fl/fl}$ mice (19–23 weeks old) with infiltrations of lymphocytes and myeloid cells observed in various organs (Fig. 1h). Thus, Atg7 is essential for T_{reg} cell-mediated immune homeostasis.

As autoimmune disease is frequently associated with loss of T_{reg} cells, we examined T_{reg} cells in the lymphoid organs of *Foxp3*^{Cre}*Atg7*$^{fl/fl}$ mice. T_{reg} cell percentages were significantly reduced in spleen, PLNs and mesenteric lymph nodes (MLNs), but not the thymus, although T_{reg} cell numbers remained largely unaltered due to the increase of total T cells (Fig. 1i). A more severe reduction of T_{reg} cells was observed in colon lamina propria, a representative site of T_{reg} activation, even in very young *Foxp3*^{Cre}*Atg7*$^{fl/fl}$ mice (Supplementary Fig. 1e). We next investigated whether T_{reg} cell reduction in *Foxp3*^{Cre}*Atg7*$^{fl/fl}$ mice was a cell-autonomous defect. We generated mixed bone marrow (BM) chimeras by reconstituting *Rag1*$^{-/-}$ mice with BM cells from CD45.1^{+} mice mixed 1:1 with those from either *Foxp3*^{Cre}*Atg7*$^{+/fl}$ or *Foxp3*^{Cre}*Atg7*$^{fl/fl}$ CD45.2^{+} mice. Atg7-deficient T_{reg} cells were underrepresented in the spleen, PLNs and MLNs, but not the thymus (Supplementary Fig. 1f), indicative of a cell-autonomous requirement of Atg7 in T_{reg} cell maintenance.

To conclusively test the role of autophagy in T_{reg} cells, we deleted another essential autophagy gene, *Atg5*, in T_{reg} cells by crossing *Atg5*$^{fl/fl}$ mice with *Foxp3*$^{YFP\text{-}Cre}$ mice (*Foxp3*^{Cre}*Atg5*$^{fl/fl}$). *Foxp3*^{Cre}*Atg5*$^{fl/fl}$ mice had disrupted immune homeostasis of CD4^{+} and CD8^{+} cells (Supplementary Fig. 1g), associated with increased IFN-γ expression (Supplementary Fig. 1h). Additionally, *Foxp3*^{Cre}*Atg5*$^{fl/fl}$ mice had reduced T_{reg} cell percentage (Supplementary Fig. 1i). Therefore, these results establish autophagy as a central and intrinsic regulator of T_{reg} cell maintenance and immune homeostasis.

Impaired survival and stability of Atg7-null T_{reg} cells

To investigate the underlying basis for the reduced cellularity of Atg7-deficient T_{reg} cells, we first examined T_{reg} cell proliferation. T_{reg} cells in *Foxp3*^{Cre}*Atg7*$^{fl/fl}$ mice actually contained a higher percentage of Ki67^{+} cells than those in *Foxp3*^{Cre}*Atg7*$^{+/fl}$ mice (Supplementary Fig. 2a), but Atg7-deficient T_{reg} cells from the mixed BM chimeras had normal percentage of Ki67^{+} cells (Supplementary Fig. 2b). Moreover, *Foxp3*^{Cre}*Atg7*$^{+/fl}$ and *Foxp3*^{Cre}*Atg7*$^{fl/fl}$ T_{reg} cells showed comparable proliferation after *in vitro* stimulation or adoptive transfer into *Rag1*$^{-/-}$ mice (Supplementary Fig. 2c,d). Thus, Atg7 is dispensable for T_{reg} cell proliferation, and the reduced T_{reg} cellularity in the absence of Atg7 is unlikely to result from a proliferative defect.

Because peripheral T_{reg} cell number is tightly regulated by apoptosis[11], we next examined apoptosis of T_{reg} cells. T_{reg} cells in *Foxp3*^{Cre}*Atg7*$^{fl/fl}$ mice had greatly increased staining of active caspase-3 as compared to those in *Foxp3*^{Cre}*Atg7*$^{+/fl}$ mice (Fig. 2a), indicative of a higher rate of apoptosis. Additionally, upon *in vitro* stimulation, Atg7-deficient T_{reg} cells were impaired in survival, as indicated by the increased staining with active caspase-3 and 7-AAD (Fig. 2b), and upregulation of Bim, which initiates T_{reg} apoptosis[11] (Fig. 2c). Atg7-deficient T_{reg} cells from mixed BM chimeras also had increased active caspase-3 and Bim expression (Supplementary Fig. 2e,f), indicative of a cell-autonomous requirement of Atg7 in T_{reg} cell survival.

Aside from cell survival, lineage stability of T_{reg} cells is crucial for their maintenance and function[7–10]. Although mean fluorescence intensity (MFI) of Foxp3 was comparable in Atg7-sufficient and deficient T_{reg} cells (data not shown), T_{reg} cells from *Foxp3*^{Cre}*Atg7*$^{fl/fl}$

mice had significantly elevated expression of IFN-γ under steady state (Fig. 2d), and upon tumor inoculation (Supplementary Fig. 2g). To directly examine the role of autophagy in maintaining Foxp3 expression in activated T_{reg} cells *in vivo*, we transferred Atg7-sufficient and deficient T_{reg} cells into *Rag1*$^{-/-}$ mice and assessed Foxp3 expression at 7–10 days after transfer. While only a small proportion of Atg7-sufficient T_{reg} cells lost Foxp3 expression following homeostatic proliferation, the majority of Atg7-deficient T_{reg} cells were unable to maintain Foxp3 (Fig. 2e). Loss of Foxp3 expression in Atg7-deficient T_{reg} cells was associated with acquisition of production of IFN-γ, and to a lesser extent, IL-17 (Fig. 2f). IFN-γ expression was also elevated in the residual Foxp3^{+} T_{reg} cells deficient in Atg7 (Fig. 2f). Moreover, in an *in vitro* system to measure stability of activated T_{reg} cells[22,23], Atg7-deficient T_{reg} cells had greatly reduced Foxp3 (Fig. 2g) and elevated IFN-γ expression (Supplementary Fig. 2h). Collectively, T_{reg} cells lacking Atg7 show impaired Foxp3 expression but aberrant acquisition of inflammatory cytokine expression *in vivo* and *in vitro*, indicating a central role of autophagy in maintaining the stability of T_{reg} cells.

To explore the relationship between survival and stability defects of Atg7-deficient T_{reg} cells, we crossed *Foxp3*^{Cre}*Atg7*$^{fl/fl}$ mice with mice expressing a *Bcl2* transgene in lymphocytes (*Bcl2*-transgenic, *Bcl2*-TG)[24]. The excessive apoptosis of *Foxp3*^{Cre}*Atg7*$^{fl/fl}$ T_{reg} cells was reduced in *Foxp3*^{Cre}*Atg7*$^{fl/fl}$*Bcl2*-TG cells (Supplementary Fig. 2i). However, *Foxp3*^{Cre}*Atg7*$^{fl/fl}$*Bcl2*-TG mice still had reduced T_{reg} cell percentage and spontaneously activated conventional T cells (Supplementary Fig. 2j,k). Additionally, as compared with T_{reg} cells from control *Bcl2*-TG mice, those from *Foxp3*^{Cre}*Atg7*$^{fl/fl}$*Bcl2*-TG mice had elevated expression of IFN-γ (Supplementary Fig. 2l), and reduced Foxp3 expression after *in vitro* culture (Supplementary Fig. 2m). Therefore, survival and stability defects of Atg7-deficient T_{reg} cells represent two discrete effects induced by loss of autophagy.

Atg7 restricts TCR-dependent mTORC1 signaling

To explore the biochemical basis for Atg7 functions, we performed functional genomics studies and found that phosphatidylinositol-3-OH kinase (PI(3)K) p110δ signaling, which was crucial for mTORC1 activation, was enhanced in *Foxp3*^{Cre}*Atg7*$^{fl/fl}$ T_{reg} cells (data not shown). Further, *Foxp3*^{Cre}*Atg7*$^{fl/fl}$ T_{reg} cells had increased cell size and CD71 and CD98 expression (Fig. 3a), all of which are dependent upon mTORC1 signaling[25]. Indeed, flow cytometry analysis showed that T_{reg} cells from *Foxp3*^{Cre}*Atg7*$^{fl/fl}$ mice had increased S6 phosphorylation, indicative of mTORC1 activation (Fig. 3a). After anti-CD3 and anti-CD28 stimulation, Atg7-deficient cells exhibited a more pronounced upregulation of S6 and 4EBP1phosphorylation, as compared with Atg7-sufficient T_{reg} cells (Fig. 3b). Furthermore, Atg5-deficient T_{reg} cells had increased cell size, CD71 and CD98 expression, and S6 phosphorylation (Supplementary Fig. 3a). Therefore, autophagy is essential for restraining mTORC1 activity in T_{reg} cells.

Signals from TCR, CD28 co-stimulation and IL-2 elicit mTORC1 activity[26]. To investigate the involvements of upstream inputs for mTORC1 regulation, we activated T_{reg} cells with different stimuli and measured S6 phosphorylation. Anti-CD3 stimulation resulted in hyperactivation of S6 phosphorylation in *Foxp3*^{Cre}*Atg7*$^{fl/fl}$ T_{reg} cells, and CD28 co-stimulation further boosted S6 phosphorylation in both *Foxp3*^{Cre}*Atg7*$^{+/fl}$ and

Foxp3^{Cre}*Atg7*$^{fl/fl}$ T_{reg} cells (Fig. 3c). The kinases PI(3)K, Akt and PDK1 are known to contribute to mTORC1 activation in response to TCR-CD28 stimulation[26]. To determine the molecular basis for TCR-CD28-induced aberrant mTORC1 activation in the absence of Atg7, we treated cells with inhibitors for PI(3)K (LY294002), Akt (AKTi-1/2), and PDK1 (PDKi). Inhibition of PI(3)K and PDK1, but not Akt, blocked excessive S6 phosphorylation in Atg7-deficient T_{reg} cells (Fig. 3d). Moreover, compared with control cells, Atg7-deficient T_{reg} cells had moderately increased expression of the PI(3)K components p110δ and p85, and PDK1 (Supplementary Fig. 3b), while expression of Lck or phosphorylation of total tyrosine residues including Lck was unaltered (Supplementary Fig. 3b and data not shown). These results indicate that autophagy negatively regulates PI(3)K-PDK1 abundance and activation.

To determine the contribution of aberrant mTORC1 signaling to the defects in Atg7-deficient T_{reg} cells, we treated *Foxp3*^{Cre}*Atg7*$^{fl/fl}$ mice with rapamycin *in vivo*. Rapamycin treatment moderately reduced active capase-3 staining (Fig. 3e), but more importantly, greatly diminished IFN-γ production in T_{reg} cells in *Foxp3*^{Cre}*Atg7*$^{fl/fl}$ mice (Fig. 3f). Moreover, following adoptive transfer of Atg7-sufficient and deficient T_{reg} cells into *Rag1*$^{-/-}$ mice, treatment of recipients with rapamycin largely restored Foxp3 expression in donor-derived Atg7-deficient T_{reg} cells (Fig. 3g). Rapamycin also rectified Foxp3 expression in Atg7-deficient T_{reg} cells in the *in vitro* T_{reg} cell stability assay (Fig. 3h). Therefore, autophagy maintains T_{reg} cell stability, at least in part, by restraining mTORC1 signaling.

Atg7-mediated transcriptional programs rely on mTORC1

To explore autophagy-dependent transcriptional programs, we analyzed gene expression profiles of *in vitro* activated T_{reg} cells. Compared to *Foxp3*^{Cre}*Atg7*$^{+/fl}$ cells, expression of 360 and 398 probes were respectively upregulated and downregulated (by greater than 0.5 $\log_2$ fold change) in *Foxp3*^{Cre}*Atg7*$^{fl/fl}$ T_{reg} cells (Fig. 4a). To identify key networks regulated by autophagy in activated T_{reg} cells, we did gene-set enrichment analysis (GSEA)[27]. Consistent with our finding that Atg7-deficient T_{reg} cells had defective survival and stability, the caspase and cytokine pathways were enriched in these cells (Fig. 4b,c). Furthermore, T helper cell differentiation pathway was identified to be the most enriched canonical pathway in Atg7-deficient T_{reg} cells by ingenuity pathway analysis (IPA) of the differentially expressed genes at the 0.5 $\log_2$ cut-offs (Supplementary Fig. 4a). Also, IPA of upstream regulation revealed the activation of PI(3)K in Atg7-deficient T_{reg} cells, but suppression of Foxp3, Foxo3 and Bach2 – factors crucial for T_{reg} cell generation and maintenance by repressing effector programs[1,28,29] (Supplementary Fig. 4b). Therefore, these functional genomics analyses support a crucial role of Atg7 in restraining cytokine expression and effector programs in T_{reg} cells.

To determine the contribution of aberrant mTORC1 to Atg7-mediated transcriptional programs, we compared gene expression profiles of *in vitro* activated T_{reg} cells from *Foxp3*^{Cre}*Atg7*$^{+/fl}$ and *Foxp3*^{Cre}*Atg7*$^{fl/fl}$ mice with or without rapamycin treatment. Atg7-dependent targets (a total of 758 probes) were partitioned into five distinct clusters that differed in their responses to rapamycin (Fig. 4d). A salient feature was that the majority of Atg7 targets (493 out of 758 probes) fell into cluster 1, in which their expression was

rectified by rapamycin. Moreover, cluster 5 contained 13 probes whose expression was partially rectified by rapamycin, and cluster 2 contained 9 probes that showed the opposite direction of change in expression. Thus, ~68% (clusters 1, 2 and 5) of all Atg7 targets were rapamycin responsive as they had a diminished response after rapamycin treatment (Fig. 4d,e). In contrast, only 217 probes in cluster 4 had equal magnitude of change (> 0.5 log2 fold change) in both rapamycin-treated and non-treated *Foxp3*^{Cre}*Atg7*$^{fl/fl}$ T_{reg} cells, thus representing rapamycin non-responsive genes. In addition, cluster 3 contained 26 probes that were differentially expressed in both types of comparisons, but to a greater extent in rapamycin-treated *Foxp3*^{Cre}*Atg7*$^{fl/fl}$ T_{reg} cells compared with non-treated *Foxp3*^{Cre}*Atg7*$^{fl/fl}$ cells. Furthermore, rapamycin considerably rectified expression of genes associated with gene sets altered by Atg7 deficiency described above, namely caspase and cytokine pathways (Supplementary Fig. 4c,d). These results identify a crucial contribution of mTORC1 to autophagy-dependent transcriptional programs.

Atg7 restraints glycolytic metabolism in T_{reg} cells

Differentiation of T_{reg} cells is shaped by metabolic programs[30–32], but how T_{reg} stability is controlled by cellular metabolism remains unclear. The aberrant activation of mTORC1 in Atg7-deficient T_{reg} cells prompted us to examine the involvement of metabolic programs. We measured mitochondrial oxygen consumption rate (OCR) and extracellular acidification rate (ECAR), which denote mitochondrial OXPHOS and glycolytic activities, respectively. After TCR-CD28 stimulation, *Foxp3*^{Cre}*Atg7*$^{+/fl}$ and *Foxp3*^{Cre}*Atg7*$^{fl/fl}$ T_{reg} cells had comparable OCR (Supplementary Fig. 5a), but ECAR was significantly elevated in *Foxp3*^{Cre}*Atg7*$^{fl/fl}$ T_{reg} cells (Fig. 5a). The reduced OCR/ECAR ratio in Atg7-deficient T_{reg} cells indicated a preferential use of glycolysis over OXPHOS by these cells (Fig. 5b). Moreover, rapamycin treatment reduced ECAR in Atg7-deficient T_{reg} cells (Fig. 5c), indicating a crucial role of mTORC1 in Atg7-dependent metabolic homeostasis.

To examine the functional importance of cellular metabolism, we treated Atg7-deficient cells with dichloroacetate (DCA) in the T_{reg} stability assay; DCA shifts glycolysis towards OXPHOS by targeting pyruvate dehydrogenase kinase[30]. DCA treatment elevated Foxp3 expression in *Foxp3*^{Cre}*Atg7*$^{+/fl}$ and *Foxp3*^{Cre}*Atg7*$^{fl/fl}$ T_{reg} cells to a largely comparable level (Fig. 5d). Of note, methylation of T_{reg} cell-specific demethylated region (TSDR, also known as CNS2) is associated with maintenance of Foxp3 expression and T_{reg} cell stability[23,33]. TSDR methylation was comparable between Atg7-sufficient and deficient T_{reg} cells, and DCA treatment had no effect (Supplementary Fig. 5b). Thus, autophagy-dependent metabolic regulation contributes to Foxp3 expression but in a process independent of TSDR methylation.

To determine molecular basis for the altered glycolysis, we examined expression of hexokinase 2 (HK2), a rate-limiting enzyme in glycolysis. HK2 expression was increased in *Foxp3*^{Cre}*Atg7*$^{fl/fl}$ T_{reg} cells (Supplementary Fig. 5c), but was considerably reduced by rapamycin treatment (Supplementary Fig. 5d). In contrast, although the mTORC1-HIF1α pathway promotes glycolysis in T_H17 cells and effector $CD8^+$ T cells[32,34], HIF1α expression was not altered in Atg7-deficient T_{reg} cells (Supplementary Fig. 5e,f). Altogether, Atg7 negatively controls mTORC1-dependent glycolytic metabolism in T_{reg} cells.

c-Myc links mTORC1 to glycolysis of T_{reg} cells

Aside from HIF1α, c-Myc is another crucial regulator of T cell glycolysis[35]. c-Myc pathway was enriched in our IPA analysis of Atg7-deficient T_{reg} cells (data not shown). Compared with T_{reg} cells from *Foxp3*^{Cre}*Atg7*$^{+/fl}$ mice, those from *Foxp3*^{Cre}*Atg7*$^{fl/fl}$ T_{reg} mice had increased c-Myc expression following anti-CD3-CD28 stimulation (Fig. 6a,b). To determine if upregulation of c-Myc in Atg7-deficient T_{reg} cells depends upon mTORC1, we treated *Foxp3*^{Cre}*Atg7*$^{fl/fl}$ mice with rapamycin and examined c-Myc expression in T_{reg} cells. Rapamycin treatment considerably reduced c-Myc expression in Atg7-deficient T_{reg} cells (Fig. 6c). Moreover, dysregulated expression of c-Myc-associated genes in Atg7-deficient T_{reg} cells was rectified upon rapamycin treatment (Fig. 6d). To further explore the role of mTORC1 in mediating c-Myc expression in Atg7-deficient T_{reg} cells, we crossed *Cd4*^{Cre}*Atg7*$^{fl/fl}$ mice with *Rptor*$^{fl/fl}$ mice to abolish Raptor, the essential component of mTORC1, in Atg7-deficient T cells. Raptor deletion strongly reduced c-Myc expression in Atg7-deficient T_{reg} cells (Supplementary Fig. 6a). These results indicate that Atg7 regulates c-Myc expression in T_{reg} cells in an mTORC1-dependent manner.

The *Myc* locus is enriched with binding sites for bromodomain-containing proteins that recognize acetylated lysine residues of histones[36], and two bromodomain inhibitors, JQ-1 and i-BET-762, effectively inhibit c-Myc expression and function[36,37] (data not shown). To determine the contribution of aberrant c-Myc expression to increased glycolysis in *Foxp3*^{Cre}*Atg7*$^{fl/fl}$ T_{reg} cells, we treated cells with JQ-1 and measured ECAR. JQ-1 treatment reduced ECAR in Atg7-deficient T_{reg} cells (Fig. 6e). In the *in vitro* T_{reg} stability assay, JQ-1 or i-BET-762 restored Foxp3 expression in Atg7-deficient T_{reg} cells (Fig. 6f and Supplementary Fig. 6b). Therefore, Atg7 maintains T_{reg} cell stability by targeting mTORC1-c-Myc pathway.

Activated T_{reg} cells are sensitive to Atg7 deficiency

Under steady state, T_{reg} cells are spontaneously and continuously activated in response to self-antigens and environmental cues[3,4]. To explore the role of autophagy in T_{reg} cells with different activation states, we crossed *Foxp3*^{Cre}*Atg7*$^{fl/fl}$ mice with mice transgenic for GFP driven by the recombination-activating gene 2 (*Rag2*) promoter to label recent thymic emigrates (RTEs) with GFP[38]. In these mice, GFP$^+$ peripheral T cells represent RTEs that have left the thymus within 2–3 weeks and show naïve phenotypes, while GFP$^-$ cells are mature peripheral T cells that have experienced peripheral environment cues[3,38]. T_{reg} cells in *Rag2*^{GFP}*Foxp3*^{Cre}*Atg7*$^{fl/fl}$ mice were diminished in the GFP$^-$ compartment, but not in the GFP$^+$ compartment, as compared with the counterparts in *Rag2*^{GFP}*Foxp3*^{Cre}*Atg7*$^{+/fl}$ mice (Fig. 7a). Additionally, the increased apoptosis of Atg7-deficient T_{reg} cells, as determined by active caspase-3 staining, was observed only in the GFP$^-$ compartment (Fig. 7b). These results identify a preferential requirement of autophagy in maintaining the cellularity and survival of activated T_{reg} cells.

Published reports highlight that the activated eT_{reg} cells differentiate from the quiescent cT_{reg} population in response to environmental cues[3,4]. Autophagy activity was upregulated in eT_{reg} cells, as revealed by the significantly more GFP-LC3$^+$ puncta in eT_{reg} than cT_{reg} cells (Fig. 7c). In *Foxp3*^{Cre}*Atg7*$^{fl/fl}$ mice, the eT_{reg} population was modestly

underrepresented in T_{reg} cells (Fig. 7d), but such defect was more pronounced in a competitive environment created by the mixed BM chimeras (Fig. 7e), indicating a cell-autonomous requirement of Atg7 in this process. Moreover, eT_{reg} cells in *Foxp3*^{Cre}*Atg7*$^{fl/fl}$ mice showed a more pronounced upregulation of apoptosis compared with cT_{reg} cells (Fig. 7f). In line with this, eT_{reg} cells had higher basal level of mTORC1 activity than cT_{reg} cells as determined by S6 phosphorylation, and Atg7 deficiency augmented mTORC1 activity to a greater degree in eT_{reg} cells (Fig. 7g). Thus, autophagy functions in both T_{reg} subsets, but eT_{reg} cells are more sensitive to autophagy deficiency, in agreement with their more activated state and elevated mTORC1 activity (Supplementary Fig. 7).

Discussion

A salient feature of the autoreactive T_{reg} cells is the dynamic programming of their activation states in response to environmental and immune signals. How T_{reg} cells maintain their survival fitness and lineage stability under the activating environments is poorly understood. Here we identify that autophagy is dynamically regulated in T_{reg} cells, and deletion of Atg7 or Atg5 specifically in T_{reg} cells results in increased apoptosis and impaired lineage stability. We further reveal an inhibitory effect of autophagy on mTORC1 that contributes to the survival and stability of T_{reg} cells. Furthermore, aberrant mTORC1 elevates c-Myc expression and glycolytic metabolism in autophagy-deficient T_{reg} cells, and pharmacological blocking of excessive mTORC1, c-Myc or glycolytic activities restores, at least in part, the impaired stability of autophagy-deficient T_{reg} cells. Our studies therefore establish autophagy as a crucial regulator of T_{reg} functional integrity, and identify a key role of autophagy in restraining mTORC1 and c-Myc function and glycolytic metabolism.

Homeostatic stimuli and environmental cues drive the continuous activation and progressive functional maturation of T_{reg} cells[2]. However, after activation *in vivo* and *in vitro,* a proportion of T_{reg} cells lose Foxp3 expression and lineage stability[22,23]. One unanswered question is therefore how T_{reg} cells retain their survival fitness and functional integrity in activating contexts. Our studies identify an important role of autophagy in this process. T_{reg} cells exhibit higher autophagy activity than naïve T cells, and they further upregulate autophagy in the activated eT_{reg} subset. The exact stimuli that induce autophagy in T_{reg} cells remain to be identified. Autophagy deficiency has a more pronounced effect on the maintenance of activated T_{reg} cells than resting T_{reg} cells in the periphery under steady state, and at sites of inflammation including tumor microenvironment and colon lamina propria. Moreover, Atg7-deficient T_{reg} cells readily lose Foxp3 expression after extensive proliferation in *Rag1*$^{-/-}$ mice, or after TCR stimulation *in vitro*. These results identify a previously unappreciated mechanism that functions preferentially in activated T_{reg} cells to protect their survival fitness and lineage stability.

mTORC1 signaling is widely recognized as a negative regulator of autophagy. Specifically, in a nutrient-replete environment, activation of mTORC1 inhibits autophagy; downregulation of mTORC1 activity under nutrient deprivation facilitates the induction of autophagy[12–14]. However, prolonged starvation can result in the reactivation of mTORC1 in an autophagy-dependent manner by degradation of autolysosomal products[39]. Unexpectedly, we found that autophagy plays an important role in restricting mTORC1 activation in T_{reg}

cells activated by TCR and other stimuli. Of note, mTORC1 is a crucial regulator in T_{reg} cells, and either diminished or excessive mTORC1 disrupts T_{reg} cell suppressive functions[40,41]. The *in vivo* rapamycin treatment experiment highlights the impacts of mTORC1 dysregulation on the stability and survival of T_{reg} cells, and transcriptional programs controlled by Atg7. As for the biochemical mechanism by which autophagy regulates mTORC1 signaling, one possibility is that autophagy targets selective TCR signaling components or mTORC1 upstream regulators for degradation to modulate the strength of mTORC1 signaling. For example, a recent study indicates that autophagy shapes how TCR signals to NF-κB in effector T cells by selective degradation of Bcl-10, although the underlying mechanisms and functional outcomes are context-dependent[42]. In support of this notion, protein abundance of PI(3)K components and PDK1 are increased in the absence of autophagy, and pharmacological inhibition of PI(3)K or PDK1 blocks mTORC1 hyperactivation in Atg7-deficient T_{reg} cells. Future studies are warranted to reveal the detailed biochemical pathway by which autophagy modulates the activity of PI(3)K and PDK1 signaling.

T cell survival, proliferation and function require dynamic reprogramming of cellular metabolism[20], and glycolytic capacity and reserve are severely impaired in the *in vitro* generated T_{reg} cells compared with T_H1 and T_H17 cells[30]. How glycolytic activity is restrained in T_{reg} cells remains poorly defined, and our results identify a crucial inhibitory effect of autophagy on T_{reg} cell glycolysis. Importantly, pharmacological blocking of glycolytic metabolism or c-Myc function partly restores the defective stability of Atg7-deficient T_{reg} cells, thereby highlighting the functional contribution of dysregulated metabolism in this process. We and others have recently described a role of the phosphatase PTEN in the regulation of T cell glycolysis in T_{reg} cells[43,44]. However, PTEN mainly restricts mTORC2 but not mTORC1 activity in T_{reg} cells, and acts to control T_H1 and T_{FH} cell responses[43,44]. In contrast, Atg7-deficient T_{reg} cells show dysregulated mTORC1-c-Myc signaling and are selectively defective in controlling T_H1 cell response, without affecting T_{FH} cell responses (our unpublished observation), suggesting that T_{reg} cells employ discrete mechanisms to properly establish their metabolic programs. Interestingly, whereas our study indicates a negative role of glycolysis in the maintenance of T_{reg} cell stability, a recent study identifies that induction of T_{reg} cells from human conventional T cells is dependent on glycolysis[45], thereby highlighting context-dependent functions of glycolysis in T_{reg} cell biology.

In summary, our study has unveiled the interplay between autophagy and metabolic programming as a new mechanism to enforce T_{reg} cell functional integrity in response to immune signals. We further establish that autophagy acts as a negative regulator of mTORC1 and c-Myc function and glycolytic metabolism to maintain metabolic balance in activated T_{reg} cells. The identification of autophagy as a central signal-dependent quality control mechanism in T_{reg} cells provides new opportunities for therapeutic intervention of autoimmune diseases and cancer. From this perspective, by strengthening tumor-associated immune responses, targeting T_{reg} cell autophagy could act in synergy with strategies that block autophagy in tumor cells for added benefits in cancer therapy[13].

Online methods

Mice

Rag1$^{-/-}$ and *Rag2*^{GFP} mice[38] were purchased from the Jackson Laboratory. GFP-LC3, *Atg7*$^{fl/fl}$ and *Atg5*$^{fl/fl}$ mice were as described[21,46,47]. *Foxp3*$^{YFP\text{-}Cre}$ mice were a gift from A. Rudensky[48]. *Foxp3*^{Cre}*Atg7*$^{fl/fl}$ mice were used at 7–16 weeks old unless otherwise noted, with the age and gender-matched *Foxp3*^{Cre}*Atg7*$^{+/fl}$ mice as controls. For treatment with rapamycin, mice were injected intraperitoneally with rapamycin (4 mg per kg body weight) daily, and then analyzed five days later. BM chimeras were generated by transferring 5×10^6 T cell-depleted BM cells into sublethally irradiated (5 Gy) *Rag1*$^{-/-}$ mice. All mice were kept in a specific pathogen-free facility in the Animal Resource Center at St. Jude Children's Research Hospital. Animal protocols were approved by the Institutional Animal Care and Use Committee of St. Jude Children's Research Hospital.

Flow cytometry

For analysis of surface markers, cells were stained in PBS containing 2% (wt/vol) BSA, with anti-CD4 (RM4-5), anti-CD8α (53-6.7), anti-TCRβ (H57-597), anti-CD44 (1M7), anti-CD62L (MEL-14), anti-CD45.1 (A20), anti-CD45.2 (104), anti-CD71 (R17217), and anti-CD98 (RL388; all from eBioscience). Intracellular Foxp3 (FJK-16s), Ki67 (SolA15), IFN-γ (XMG1.2), IL-4 (11B11), IL-17 (17B7; all from eBioscience), Bim (C34C5), c-Myc (D84C12), and p-S6 (D57.2.2E; all from Cell Signaling Technology) were analyzed by flow cytometry according to the manufacturer's instructions. For intracellular cytokine staining, T cells were stimulated for 4 h with PMA plus ionomycin in the presence of monensin before intracellular staining according to the manufacturer's instructions (eBioscience). Caspase-3 activity was measured using active caspase-3 apoptosis kit (BD Biosciences). To monitor cell division, lymphocytes were labeled with CellTrace™ violet (Life Technologies). Flow cytometry data were acquired on LSRII or LSR Fortessa (BD Biosciences) and analyzed using Flowjo software (Tree Star).

Imaging and histology

Purified GFP-LC3 naïve $CD4^+$ cells and T_{reg} cells were rested in complete medium for 1 h at 37°C. Cells were harvested and fixed by 4% (vol/vol) neutral buffered paraformaldehyde solution. Images were acquired using a Zeiss Axio ObserverZ.1 microscope equipped with a CSU-22 spinning disk (Yokagawa), Delta Evole EMCCD camera (Photometrics), 100× 1.45 NA oil objective and Slidebook imaging software (3i Intelligent Imaging Innovations). Images were subsequently processed using a Laplacian filter to detect GFP-$LC3^+$ punctum objects having a minimum volume of 0.1 μm^3. Frequency of cells with GFP-$LC3^+$ puncta and number of GFP-$LC3^+$ puncta per cell were determined for each sample. For histology analysis, tissues were fixed by 10% (vol/vol) neutral buffered formalin solution, embedded in paraffin, sectioned and stained with hematoxylin and eosin, and the clinical signs of autoimmune diseases were analyzed by an experienced pathologist (P. Vogel).

Tumor model

MC38 colon adenocarcinoma cells were maintained in our laboratory and cultured in DMEM medium supplemented with 10% (vol/vol) FBS and 1% (vol/vol) penicillin-streptomycin. Gender-matched *Foxp3*^{Cre}*Atg7*$^{+/fl}$ mice and *Foxp3*^{Cre}*Atg7*$^{fl/fl}$ mice were injected subcutaneously with 2 × 10^5 MC38 colon adenocarcinoma cells in the right flank. Tumors were measured regularly with digital calipers and tumor volumes were calculated by the formula: Length × Width × [(Length × Width) ^ 0.5] × π/6. To prepare tumor infiltrating lymphocytes (TILs), tumor was excised, minced and digested with 0.5 mg/ml Collagenase IV (Roche) + 200 U/ml DNase I (Sigma) for 1 h at 37°C. TILs were isolated by density-gradient centrifugation over Percoll (Life Technologies).

Cell purification and culture

Unless otherwise noted, lymphocytes were isolated from spleen and PLNs, that included inguinal, auxiliary and cervical lymph nodes, and naïve CD4$^+$ cells (CD4$^+$Foxp3-YFP$^-$CD44^{lo}CD62L^{hi}), T_{reg} cells (CD4$^+$Foxp3-YFP$^+$), cT_{reg} cells (CD4$^+$Foxp3-YFP$^+$CD44^{lo}CD62L^{hi}) and eT_{reg} cells (CD4$^+$Foxp3-YFP$^+$CD44^{hi}CD62L^{lo}) were sorted on a MoFlow (Beckman-Coulter) or Reflection (i-Cyt). Sorted T_{reg} cells were cultured in plates coated with anti-CD3 (145-2C11) and anti-CD28 (37.51; both from eBioscience) for 4 days in Click's medium supplemented with β-mercaptoethanl, 10% (vol/vol) FBS, 1% (vol/vol) penicillin-streptomycin and 200 U/ml IL-2. In some experiments, rapamycin (50 nM), JQ-1 (500 nM), i-BET-762 (500 nM) and DCA (10 mM) were added to the culture.

Adoptive transfer

For adoptive transfer, T_{reg} cells from *Foxp3*^{Cre}*Atg7*$^{+/fl}$ mice and *Foxp3*^{Cre}*Atg7*$^{fl/fl}$ mice were transferred to the *Rag1*$^{-/-}$ mice. Seven to ten days after the transfer, recipients were euthanized for the analysis of Foxp3 and cytokine expression in transferred cells. For treatment with rapamycin, *Rag1*$^{-/-}$ mice were injected intraperitoneally with rapamycin (2 mg per kg body weight) every other day from day 1, and then analyzed at day 10.

RNA and Immunoblot analysis

Real-time PCR analysis was performed with primers and probe sets from Applied Biosystems, as described[49]. Immunoblots were performed as described previously[24], using the following antibodies: Lck (2752), HK2 (C64G5), p85 (19H8), PDK1 (3062), p-S6 (2F9), p-4EBP1 (236B4), c-Myc (D84C12; all from Cell Signaling Technology), LC3 (NB100-2220; Novus), p110δ (EPR386; Abcam), HIF1α (10006421; Cayman) and β-actin (AC-15; Sigma).

Seahorse assays

Sorted T_{reg} cells were stimulated with plate-bound anti-CD3 and anti-CD28 for 4 h in the presence of IL-2. In certain experiments, rapamycin (50 nM) and JQ-1 (500 nM) were added to the culture. After stimulation, cells were re-plated in XF media (non-buffered DMEM containing 5 mM glucose, 2 mM L-glutamine and 1 mM sodium pyruvate). XF-24 Extracellular Flux Analyzer (Seahorse Bioscience) was used to measure OCR and ECAR in

response to 1 μM oligomycin, 2 μM fluoro-carbonyl cyanide phenylhydrazone (FCCP) and 1 μM Rotenone.

Methylation analysis of T_{reg} cell-specific demethylated region

CellTrace-labeled T_{reg} cells were cultured with anti-CD3, anti-CD28, and IL-2 for 4 days in the presence of DMSO or DCA. Divided cells were sorted, and genomic DNA was prepared by a DNeasy Blood & Tissue kit (Qiagen). Bisulfite conversion of DNA was conducted with an EZ DNA Methylation-Direct kit (Zymo Research). Intron 1 of *Foxp3* (corresponding to *CNS2*) was amplified with a primer set as described (forward, 5′-TATTTTTTTGGGTTTTGGGATATTA-3′ and reverse, 5′-AACCAACCAACTTCCTACACTATCTAT-3′)[44]. PCR products were ligated into pGEM-T Easay vectors (Promega) and sequenced (more than 29 sequences per sample).

Gene expression profiling and bioinformatic analysis

T_{reg} cells from *Foxp3*^{Cre}*Atg7*$^{+/fl}$ mice (n=4), *Foxp3*^{Cre}*Atg7*$^{fl/fl}$ mice (n=4), rapamycin-treated *Foxp3*^{Cre}*Atg7*$^{+/fl}$ mice (n=4) and rapamycin-treated *Foxp3*^{Cre}*Atg7*$^{fl/fl}$ mice (n=4) were stimulated with plate-bound anti-CD3 and anti-CD28 for 4 h. RNA samples from these cells were analyzed with the Mouse Gene 2.0 ST Signals array. Differentially expressed transcripts were identified by ANOVA (Partek Genomics Suite v6.5) and the Benjamini-Hochberg method was used to estimate the false discovery rate (FDR) as described previously[25]. Lists of differentially expressed genes at the 0.5 $\log_2$ cut-offs were used for IPA canonical pathway and upstream signaling analyses. GSEA was performed as described[27]. The microarray data have been deposited into the GEO series database (GSE75218).

Statistical analysis

Prism 5 software (GraphPad) was used to analyze data by performing two-tail unpaired Student's *t*-test. When multiple groups were compared, one-way ANOVA with the Tukey test was performed. *P* value of less than 0.05 was considered significant. All error bars represent the s.e.m.

Supplementary Material

Refer to Web version on PubMed Central for supplementary material.

Acknowledgments

The authors acknowledge B. Rhode, C. Cloer and S. Rankin for animal colony management, X. Du for help with immunoblot analysis, N. Kalupahana for initial analysis of Atg7-deficient mice, A. Rudensky for *Foxp3*$^{YFP-Cre}$ mice, J.E. Bradner for providing the JQ-1 compound, St. Jude Immunology FACS core facility for cell sorting, and Y. Wang for editing. This work was supported by US National Institutes of Health (NIH AI105887, AI101407, CA176624 and NS064599), and Crohn's and Colitis Foundation of America (to H.C.).

References

1. Josefowicz SZ, Lu LF, Rudensky AY. Regulatory T Cells: Mechanisms of Differentiation and Function. Annu Rev Immunol. 2012; 30:531–564. [PubMed: 22224781]

2. Liston A, Gray DHD. Homeostatic control of regulatory T cell diversity. Nat Rev Immunol. 2014; 14:154–165. [PubMed: 24481337]
3. Smigiel KS, et al. CCR7 provides localized access to IL-2 and defines homeostatically distinct regulatory T cell subsets. J Exp Med. 2014; 211:121–136. [PubMed: 24378538]
4. Fisson S, et al. Continuous activation of autoreactive CD4+ CD25+ regulatory T cells in the steady state. J Exp Med. 2003; 198:737–746. [PubMed: 12939344]
5. Arvey A, et al. Inflammation-induced repression of chromatin bound by the transcription factor Foxp3 in regulatory T cells. Nat Immunol. 2014; 15:580–587. [PubMed: 24728351]
6. Rubtsov YP, et al. Stability of the Regulatory T Cell Lineage in Vivo. Science. 2010; 329:1667–1671. [PubMed: 20929851]
7. Zhou XY, et al. Instability of the transcription factor Foxp3 leads to the generation of pathogenic memory T cells in vivo. Nat Immunol. 2009; 10:1000–1007. [PubMed: 19633673]
8. Bailey-Bucktrout SL, et al. Self-antigen-Driven Activation Induces Instability of Regulatory T Cells during an Inflammatory Autoimmune Response. Immunity. 2013; 39:949–962. [PubMed: 24238343]
9. Komatsu N, et al. Pathogenic conversion of Foxp3(+) T cells into T(H)17 cells in autoimmune arthritis. Nat Med. 2014; 20:62–68. [PubMed: 24362934]
10. Tsuji M, et al. Preferential generation of follicular B helper T cells from Foxp3+ T cells in gut Peyer's patches. Science. 2009; 323:1488–1492. [PubMed: 19286559]
11. Pierson W, et al. Antiapoptotic Mcl-1 is critical for the survival and niche-filling capacity of Foxp3(+) regulatory T cells. Nat Immunol. 2013; 14:959–965. [PubMed: 23852275]
12. Levine B, Mizushima N, Virgin HW. Autophagy in immunity and inflammation. Nature. 2011; 469:323–335. [PubMed: 21248839]
13. Jiang X, Overholtzer M, Thompson CB. Autophagy in cellular metabolism and cancer. J Clin Invest. 2015; 125:47–54. [PubMed: 25654550]
14. Galluzzi L, Pietrocola F, Levine B, Kroemer G. Metabolic control of autophagy. Cell. 2014; 159:1263–1276. [PubMed: 25480292]
15. Pua HH, Dzhagalov I, Chuck M, Mizushima N, He YW. A critical role for the autophagy gene Atg5 in T cell survival and proliferation. J Exp Med. 2007; 204:25–31. [PubMed: 17190837]
16. Xu X, et al. Autophagy is essential for effector CD8(+) T cell survival and memory formation. Nat Immunol. 2014; 15:1152–1161. [PubMed: 25362489]
17. Hubbard VM, et al. Macroautophagy regulates energy metabolism during effector T cell activation. J Immunol. 2010; 185:7349–7357. [PubMed: 21059894]
18. Li C, et al. Autophagy is induced in CD4+ T cells and important for the growth factor-withdrawal cell death. J Immunol. 2006; 177:5163–5168. [PubMed: 17015701]
19. Pengo N, et al. Plasma cells require autophagy for sustainable immunoglobulin production. Nat Immunol. 2013; 14:298–305. [PubMed: 23354484]
20. MacIver NJ, Michalek RD, Rathmell JC. Metabolic regulation of T lymphocytes. Annu Rev Immunol. 2013; 31:259–283. [PubMed: 23298210]
21. Mizushima N, Yamamoto A, Matsui M, Yoshimori T, Ohsumi Y. In vivo analysis of autophagy in response to nutrient starvation using transgenic mice expressing a fluorescent autophagosome marker. Mol Biol Cell. 2004; 15:1101–1111. [PubMed: 14699058]
22. Li X, Liang Y, LeBlanc M, Benner C, Zheng Y. Function of a Foxp3 cis-element in protecting regulatory T cell identity. Cell. 2014; 158:734–748. [PubMed: 25126782]
23. Feng Y, et al. Control of the inheritance of regulatory T cell identity by a cis element in the Foxp3 locus. Cell. 2014; 158:749–763. [PubMed: 25126783]
24. Liu G, Yang K, Burns S, Shrestha S, Chi H. The S1P(1)-mTOR axis directs the reciprocal differentiation of T(H)1 and T(reg) cells. Nat Immunol. 2010; 11:1047–1056. [PubMed: 20852647]
25. Yang K, et al. T cell exit from quiescence and differentiation into Th2 cells depend on Raptor-mTORC1-mediated metabolic reprogramming. Immunity. 2013; 39:1043–1056. [PubMed: 24315998]

26. Chi H. Regulation and function of mTOR signalling in T cell fate decisions. Nat Rev Immunol. 2012; 12:325–338. [PubMed: 22517423]
27. Subramanian A, et al. Gene set enrichment analysis: a knowledge-based approach for interpreting genome-wide expression profiles. Proc Natl Acad Sci USA. 2005; 102:15545–15550. [PubMed: 16199517]
28. Roychoudhuri R, et al. BACH2 represses effector programs to stabilize T(reg)-mediated immune homeostasis. Nature. 2013; 498:506–510. [PubMed: 23728300]
29. Ouyang W, et al. Foxo proteins cooperatively control the differentiation of Foxp3+ regulatory T cells. Nat Immunol. 2010; 11:618–627. [PubMed: 20467422]
30. Gerriets VA, et al. Metabolic programming and PDHK1 control CD4+ T cell subsets and inflammation. J Clin Invest. 2015; 125:194–207. [PubMed: 25437876]
31. Michalek RD, et al. Cutting edge: distinct glycolytic and lipid oxidative metabolic programs are essential for effector and regulatory CD4+ T cell subsets. J Immunol. 2011; 186:3299–3303. [PubMed: 21317389]
32. Shi LZ, et al. HIF1alpha-dependent glycolytic pathway orchestrates a metabolic checkpoint for the differentiation of TH17 and Treg cells. J Exp Med. 2011; 208:1367–1376. [PubMed: 21708926]
33. Polansky JK, et al. DNA methylation controls Foxp3 gene expression. Eur J Immunol. 2008; 38:1654–1663. [PubMed: 18493985]
34. Finlay DK, et al. PDK1 regulation of mTOR and hypoxia-inducible factor 1 integrate metabolism and migration of CD8+ T cells. J Exp Med. 2012; 209:2441–2453. [PubMed: 23183047]
35. Wang R, et al. The transcription factor Myc controls metabolic reprogramming upon T lymphocyte activation. Immunity. 2011; 35:871–882. [PubMed: 22195744]
36. Delmore JE, et al. BET Bromodomain Inhibition as a Therapeutic Strategy to Target c-Myc. Cell. 2011; 146:903–916.
37. Bandukwala HS, et al. Selective inhibition of CD4+ T-cell cytokine production and autoimmunity by BET protein and c-Myc inhibitors. Proc Natl Acad Sci USA. 2012; 109:14532–14537. [PubMed: 22912406]
38. Boursalian TE, Golob J, Soper DM, Cooper CJ, Fink PJ. Continued maturation of thymic emigrants in the periphery. Nat Immunol. 2004; 5:418–425. [PubMed: 14991052]
39. Yu L, et al. Termination of autophagy and reformation of lysosomes regulated by mTOR. Nature. 2010; 465:942–946. [PubMed: 20526321]
40. Zeng H, et al. mTORC1 couples immune signals and metabolic programming to establish T(reg)-cell function. Nature. 2013; 499:485–490. [PubMed: 23812589]
41. Park Y, et al. TSC1 regulates the balance between effector and regulatory T cells. J Clin Invest. 2013; 123:5165–5178. [PubMed: 24270422]
42. Paul S, Kashyap AK, Jia W, He YW, Schaefer BC. Selective autophagy of the adaptor protein Bcl10 modulates T cell receptor activation of NF-kappaB. Immunity. 2012; 36:947–958. [PubMed: 22658522]
43. Shrestha S, et al. Treg cells require the phosphatase PTEN to restrain TH1 and TFH cell responses. Nat Immunol. 2015; 16:178–187. [PubMed: 25559258]
44. Huynh A, et al. Control of PI(3) kinase in Treg cells maintains homeostasis and lineage stability. Nat Immunol. 2015; 16:188–196. [PubMed: 25559257]
45. De Rosa V, et al. Glycolysis controls the induction of human regulatory T cells by modulating the expression of FOXP3 exon 2 splicing variants. Nat Immunol. 2015; 16:1174–1184. [PubMed: 26414764]
46. Kuma A, et al. The role of autophagy during the early neonatal starvation period. Nature. 2004; 432:1032–1036. [PubMed: 15525940]
47. Hara T, et al. Suppression of basal autophagy in neural cells causes neurodegenerative disease in mice. Nature. 2006; 441:885–889. [PubMed: 16625204]
48. Rubtsov YP, et al. Reaulatory T cell-derived interleukin-10 limits inflammation at environmental interfaces. Immunity. 2008; 28:546–558. [PubMed: 18387831]
49. Wang Y, et al. Tuberous sclerosis 1 (Tsc1)-dependent metabolic checkpoint controls development of dendritic cells. Proc Natl Acad Sci USA. 2013; 110:E4894–4903. [PubMed: 24282297]

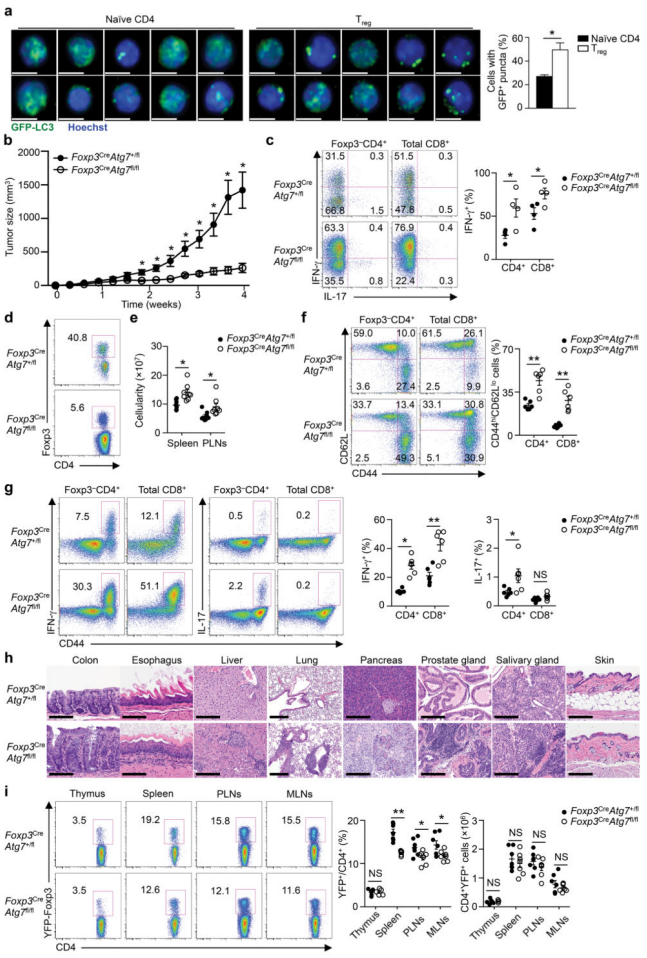

Figure 1. T_{reg} cells have active autophagy and require Atg7 for mediating tumor immune tolerance and self-tolerance

(**a**) Representative images (scale bars, 5 μm) (left) and quantification of percentages of cells with GFP-LC3$^+$ puncta (right) in peripheral naïve CD4$^+$ cells and T_{reg} cells purified from GFP-LC3 mice (n=3 mice). (**b–d**) *Foxp3*^{Cre}*Atg7*$^{+/fl}$ and *Foxp3*^{Cre}*Atg7*$^{fl/fl}$ mice (n=4 mice per genotype) were inoculated with MC38 colon adenocarcinoma cells, and tumor growth (**b**) was measured. Flow cytometry analyzing IFN-γ expression in Foxp3$^-$CD4$^+$ and CD8$^+$ T cells (**c**, left), frequency of IFN-γ$^+$ cells (**c**, right) and Foxp3 expression in CD4$^+$ T cells (**d**) in tumor-infiltrating lymphocytes. Numbers in quadrants indicate percent cells in each throughout, and numbers adjacent to outlined areas indicate percent Foxp3$^+$ cells (**d**). (**e–g**) Analysis of *Foxp3*^{Cre}*Atg7*$^{+/fl}$ and *Foxp3*^{Cre}*Atg7*$^{fl/fl}$ mice (10–12 weeks old) under steady state. Total cellularity of spleen and PLNs (n=8 mice per genotype) (**e**). Flow cytometry analyzing the expression of CD62L and CD44 (**f**, left) and IFN-γ and IL-17 (**g**, left), and frequency of CD44^{hi}CD62L^{lo} cells (n=6 mice per genotype) (**f**, right) and IFN-γ$^+$ or IL-17$^+$ cells (n=6 mice per genotype) (**g**, right) in splenic Foxp3$^-$CD4$^+$ and CD8$^+$ T cells. Numbers adjacent to outlined areas indicate percent IFN-γ$^+$ or IL-17$^+$ cells (**g**, left). (**h**) Hematoxylin and eosin staining of colon, esophagus, liver, lung, pancreas, prostate gland, salivary gland, and skin from *Foxp3*^{Cre}*Atg7*$^{+/fl}$ and *Foxp3*^{Cre}*Atg7*$^{fl/fl}$ mice (19–23 weeks old). Magnification and scale bars: ×40 and 100 μm (colon and skin), ×20 and 200 μm

(esophagus, liver, pancreas, prostate gland and salivary gland) and ×10 and 200 μm (lung). (**i**) Flow cytometry analyzing YFP-Foxp3 expression in $CD4^+$ T cells (left), and frequency and number of YFP-$Foxp3^+$ cells (right) in the thymus, spleen, PLNs and mesenteric lymph nodes (MLNs) of $Foxp3^{Cre}Atg7^{+/fl}$ and $Foxp3^{Cre}Atg7^{fl/fl}$ mice (10–12 weeks old) (n=7 mice per genotype). Numbers adjacent to outlined areas indicate percent YFP-$Foxp3^+$ cells (**g**, left). NS, not significant ($P > 0.05$); * $P < 0.05$ and ** $P < 0.001$ (two-tail unpaired Student's *t*-test in **a-c,e–g,i**). Data are representative of two (**a–d,h**) experiments, or pooled from five out of six (**e**), four out of six (**f,g**) or three out of six (**i**) experiments (mean ± s.e.m in **a–c,e–g,i**).

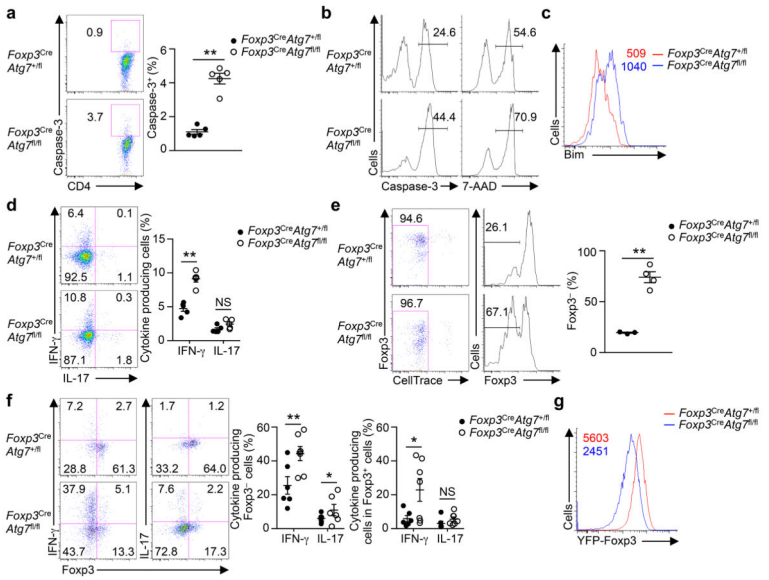

Figure 2. Atg7 contributes to T_{reg} cell survival and lineage stability

(**a**) Flow cytometry analyzing active caspase-3 expression (left), and frequency of caspase-3$^+$ cells (right) in T_{reg} cells from the spleen of *Foxp3*^{Cre}*Atg7*$^{+/fl}$ and *Foxp3*^{Cre}*Atg7*$^{fl/fl}$ mice (n=5 mice per genotype). Numbers adjacent to outlined areas indicate percent caspase-3$^+$ cells (left). (**b,c**) Flow cytometry analyzing active caspase-3 expression and 7-AAD staining (**b**) and Bim expression (**c**) in T_{reg} cells (from *Foxp3*^{Cre}*Atg7*$^{+/fl}$ and *Foxp3*^{Cre}*Atg7*$^{fl/fl}$ mice) stimulated with anti-CD3, anti-CD28, and IL-2 for overnight. Numbers above bracketed lines indicate percent caspase-3$^+$ or 7-AAD$^+$ cells (**b**), and numbers above graph indicate mean fluorescence intensity (MFI) of Bim (**c**). (**d**) Flow cytometry analyzing the expression of IFN-γ and IL-17 (left), and frequency of IFN-γ$^+$ cells and IL-17$^+$ cells (right) in splenic T_{reg} cells from *Foxp3*^{Cre}*Atg7*$^{+/fl}$ and *Foxp3*^{Cre}*Atg7*$^{fl/fl}$ mice (n=5 mice per genotype). Numbers in quadrants indicate percent cells in each throughout. (**e,f**) T_{reg} cells (sorted from *Foxp3*^{Cre}*Atg7*$^{+/fl}$ and *Foxp3*^{Cre}*Atg7*$^{fl/fl}$ mice) were transferred into *Rag1*$^{-/-}$ mice. Flow cytometry analyzing CellTrace dilution (**e**, left) and the expression of Foxp3 (**e**, left) and IFN-γ and IL-17 (**f**, left), and frequency of Foxp3$^-$ cells (**e**, right) (n=3 mice for *Atg7*$^{+/fl}$ and n=4 mice for *Atg7*$^{fl/fl}$) and IFN-γ$^+$ cells and IL-17$^+$ cells (**f**, right) (n=6 mice for *Atg7*$^{+/fl}$ and n=7 mice for *Atg7*$^{fl/fl}$) in divided CellTrace-labeled donor cells (gated on CD4$^+$TCRβ$^+$). Numbers adjacent to outlined areas indicate percent CellTrace^{lo} cells (**e**, left), and numbers above bracketed lines indicate percent Foxp3$^-$ cells (**e**, left). (**g**) Flow cytometry analyzing YFP-Foxp3 expression in divided T_{reg} cells (from *Foxp3*^{Cre}*Atg7*$^{+/fl}$ and *Foxp3*^{Cre}*Atg7*$^{fl/fl}$ mice) that were activated *in vitro* with anti-CD3, anti-CD28 and IL-2 for 96 h. Numbers above graphs indicate MFI of YFP-Foxp3. NS, not significant ($P > 0.05$); * $P < 0.05$ and ** $P < 0.001$ (two-tail unpaired Student's *t*-test in **a,d–f**). Data are pooled from two out of five (**a**), four out of ten (**d**) or two out of two (**f**) experiments, or representative of three (**b,c**), ten (**e**) or five (**g**) experiments (mean ± s.e.m in **a,d–f**).

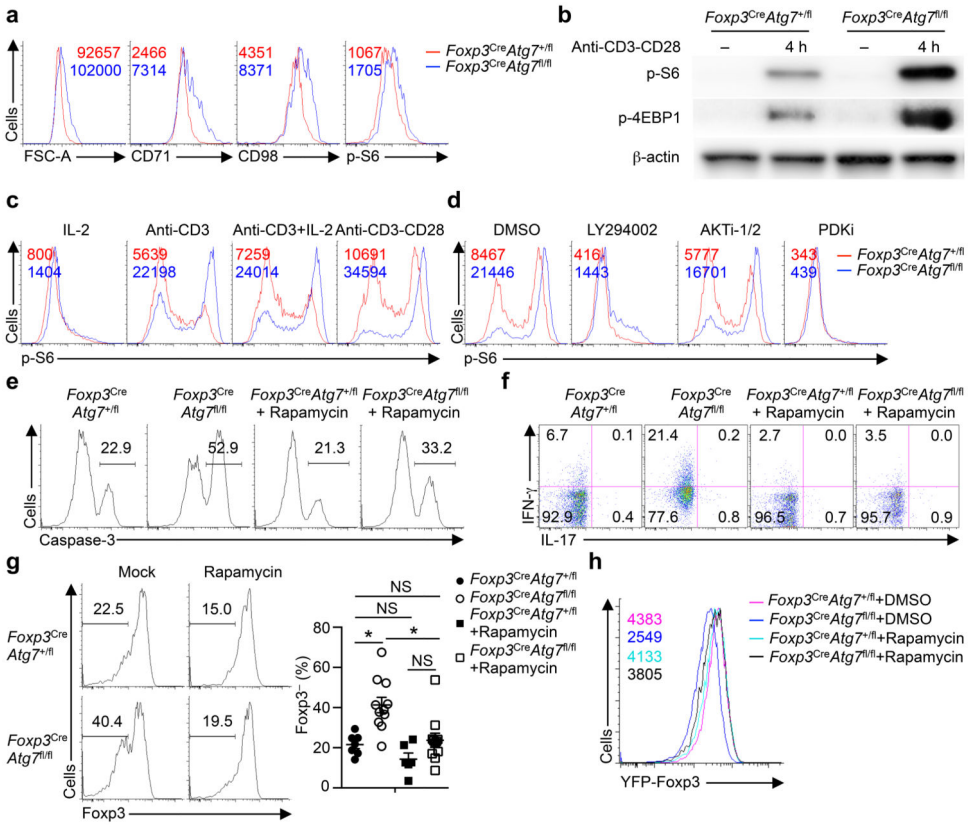

Figure 3. Atg7 restrains TCR-dependent mTORC1 activity in T_{reg} cells

(**a**) Flow cytometry analyzing cell size, and the expression of CD71, CD98 and p-S6 in *Foxp3*^{Cre}*Atg7*$^{+/fl}$ and *Foxp3*^{Cre}*Atg7*$^{fl/fl}$ splenic T_{reg} cells. Numbers above graphs indicate MFI of FSC-A, CD71, CD98 or p-S6. (**b**) Immunoblot analysis of p-S6 and p-4EBP1 in resting, and anti-CD3 and antiCD28-stimulated T_{reg} cells from *Foxp3*^{Cre}*Atg7*$^{+/fl}$ and *Foxp3*^{Cre}*Atg7*$^{fl/fl}$ mice. (**c**) Flow cytometry analyzing p-S6 expression in *Foxp3*^{Cre}*Atg7*$^{+/fl}$ and *Foxp3*^{Cre}*Atg7*$^{fl/fl}$ T_{reg} cells stimulated with the indicated stimuli for 4 h. Numbers above graphs indicate MFI of p-S6. (**d**) Flow cytometry analyzing p-S6 expression in *Foxp3*^{Cre}*Atg7*$^{+/fl}$ and *Foxp3*^{Cre}*Atg7*$^{fl/fl}$ T_{reg} cells stimulated with anti-CD3 and anti-CD28 for 4 h in the presence of DMSO, LY294002 (10 μM), AKTi-1/2 (1 μM) or PDKi (10 μM). Numbers above graphs indicate MFI of p-S6. (**e,f**) *Foxp3*^{Cre}*Atg7*$^{+/fl}$ and *Foxp3*^{Cre}*Atg7*$^{fl/fl}$ mice received mock or rapamycin treatment. T_{reg} cells were isolated and stimulated overnight with anti-CD3, anti-CD28, and IL-2 for analysis of caspase-3 activity (**e**) or stimulated for 4 h for analysis of IFN-γ and IL-17 expression (**f**). Numbers above bracketed lines indicate percent caspase-3^{+} cells (**e**), and numbers in quadrants indicate percent cells in each (**f**). (**g**) *Foxp3*^{Cre}*Atg7*$^{+/fl}$ or *Foxp3*^{Cre}*Atg7*$^{fl/fl}$ T_{reg} cells were transferred into *Rag1*$^{-/-}$ mice, followed by mock (n=7 mice for *Atg7*$^{+/fl}$ and n=11 mice for *Atg7*$^{fl/fl}$) or rapamycin (n=6 mice for *Atg7*$^{+/fl}$ and n=11 mice for *Atg7*$^{fl/fl}$) treatment. Flow cytometry analyzing Foxp3 expression (left), and frequency of Foxp3^{-} cells (right) in divided donor cells (gated on CD4^{+}TCRβ^{+}) in the PLNs of recipients. Numbers above bracketed lines indicate percent Foxp3^{-} cells. (**h**) Flow cytometry analyzing YFP-Foxp3 expression in divided T_{reg} cells from *Foxp3*^{Cre}*Atg7*$^{+/fl}$ and *Foxp3*^{Cre}*Atg7*$^{fl/fl}$ mice, following DMSO or rapamycin treatment

and activation with anti-CD3, anti-CD28, and IL-2 *in vitro* for 96 h. NS, not significant ($P > 0.05$); * $P < 0.05$ (one-way ANOVA in **g**). Data are representative of three (**a,b,d–f,h**) or two (**c**) experiments, or pooled from three out of three (**g**) experiments (mean ± s.e.m in **g**).

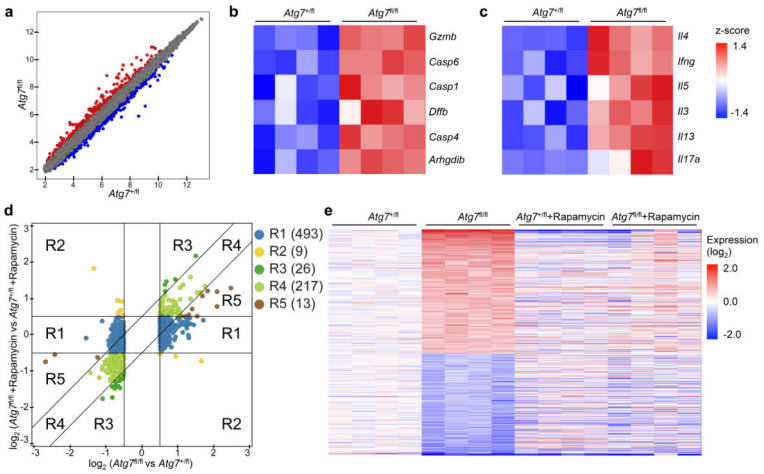

Figure 4. mTORC1 signaling is critical for Atg7-dependent transcriptional program

Foxp3^{Cre}*Atg7*$^{+/fl}$ and *Foxp3*^{Cre}*Atg7*$^{fl/fl}$ mice were treated with or without rapamycin (n=4 mice per group). T_{reg} cells were sorted and activated with anti-CD3 and anti-CD28 for 4 h for gene expression profiling. (**a**) Scatterplot comparing global gene-expression profiles between *Foxp3*^{Cre}*Atg7*$^{+/fl}$ and *Foxp3*^{Cre}*Atg7*$^{fl/fl}$ T_{reg} cells. Transcripts with > 0.5 log_2 fold increased (360 probes) or decreased (398 probes) expression in *Foxp3*^{Cre}*Atg7*$^{fl/fl}$ T_{reg} cells are shown in red or blue respectively. (**b,c**) GSEA reveals that caspase (**b**) and cytokine pathways (**c**) are among the most extensively upregulated pathways in *Foxp3*^{Cre}*Atg7*$^{fl/fl}$ T_{reg} cells as compared with *Foxp3*^{Cre}*Atg7*$^{+/fl}$ T_{reg} cells. Heat maps of top hit genes in caspase (**b**) and cytokine (**c**) pathways. Differentially expressed genes were normalized by z-score. Expression levels are shown as green for low intensities, and red for high intensities. (**d**) Comparison of expression changes in rapamycin-treated *Foxp3*^{Cre}*Atg7*$^{fl/fl}$ versus *Foxp3*^{Cre}*Atg7*$^{+/fl}$ T_{reg} cells with those in non-treated *Foxp3*^{Cre}*Atg7*$^{fl/fl}$ versus *Foxp3*^{Cre}*Atg7*$^{+/fl}$ T_{reg} cells. The 758 Atg7 target genes (with > 0.5 log_2 fold change) were partitioned into five main clusters, shown and colored by regions (R1–R5). Right, numbers indicate the number of probes within each region. (**e**) Heat maps of 515 rapamycin responsive genes that are differentially expressed in *Foxp3*^{Cre}*Atg7*$^{fl/fl}$ T_{reg} cells (with > 0.5 log_2 fold change) and have diminished response after rapamycin treatment. Red color denotes upregulated genes in *Foxp3*^{Cre}*Atg7*$^{fl/fl}$ T_{reg} cells, and blue color denotes downregulated genes in *Foxp3*^{Cre}*Atg7*$^{fl/fl}$ T_{reg} cells. Data are from one experiment (**a–e**).

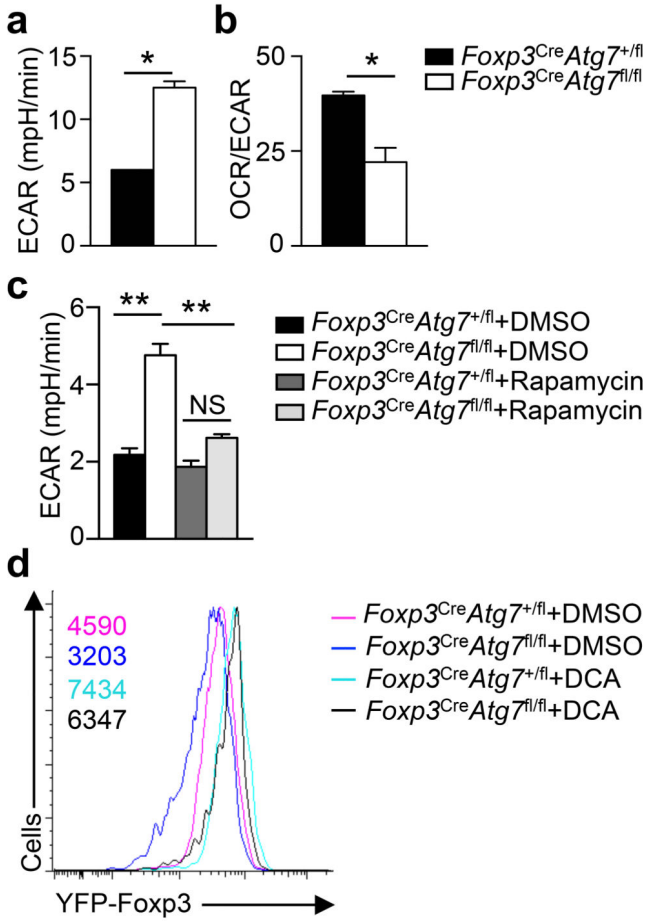

Figure 5. Dysregulation of glycolytic metabolism in Atg7-deficient T_{reg} cells contributes to impaired T_{reg} cell stability

(**a**) Measurement of ECAR in T_{reg} cells (from *Foxp3*^{Cre}*Atg7*$^{+/fl}$ and *Foxp3*^{Cre}*Atg7*$^{fl/fl}$ mice) stimulated with anti-CD3 and anti-CD28 for 4 h. (**b**) Ratio of OCR to ECAR of T_{reg} cells (from *Foxp3*^{Cre}*Atg7*$^{+/fl}$ and *Foxp3*^{Cre}*Atg7*$^{fl/fl}$ mice) stimulated with anti-CD3 and anti-CD28 for 4 h. (**c**) Measurement of ECAR in T_{reg} cells (from *Foxp3*^{Cre}*Atg7*$^{+/fl}$ and *Foxp3*^{Cre}*Atg7*$^{fl/fl}$ mice) stimulated with anti-CD3 and anti-CD28 for 4 h in the presence of DMSO or rapamycin. (**d**) Flow cytometry analyzing YFP-Foxp3 expression in divided T_{reg} cells (from *Foxp3*^{Cre}*Atg7*$^{+/fl}$ and *Foxp3*^{Cre}*Atg7*$^{fl/fl}$ mice) that were activated *in vitro* with anti-CD3, anti-CD28, and IL-2 for 96 h in the presence of DMSO or DCA. Numbers above graphs indicate MFI of YFP-Foxp3. NS, not significant ($P > 0.05$); * $P < 0.05$ and ** $P < 0.001$ (two-tail unpaired Student's *t*-test in **a,b** and one-way ANOVA in **c**). Data are representative of two (**a,b**), three (**c**) or four (**d**) experiments (mean ± s.e.m in **a–c**).

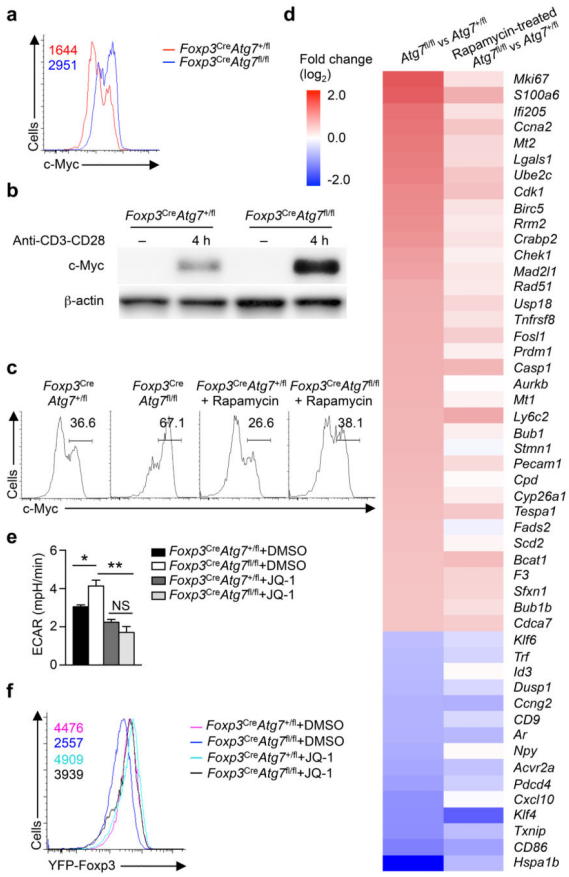

Figure 6. Autophagy protects T_{reg} cell stability by restraining mTORC1-dependent c-Myc expression and function

(**a**) Flow cytometry analyzing c-Myc in T_{reg} cells (from *Foxp3*^{Cre}*Atg7*$^{+/fl}$ and *Foxp3*^{Cre}*Atg7*$^{fl/fl}$ mice) activated with anti-CD3 and anti-CD28 for 4 h. Numbers above graphs indicate MFI of c-Myc. (**b**) Immunoblot analysis of c-Myc in resting, and anti-CD3 and anti-CD28 stimulated T_{reg} cells from *Foxp3*^{Cre}*Atg7*$^{+/fl}$ and *Foxp3*^{Cre}*Atg7*$^{fl/fl}$ mice. (**c,d**) *Foxp3*^{Cre}*Atg7*$^{+/fl}$ and *Foxp3*^{Cre}*Atg7*$^{fl/fl}$ mice received mock or rapamycin treatment. T_{reg} cells were isolated and stimulated with anti-CD3 and anti-CD28 for 4 h for analysis of c-Myc expression (**c**). Numbers above bracketed lines indicate percent c-Myc^{+} cells (**c**). Heat maps of Myc target gene expression in non-treated *Foxp3*^{Cre}*Atg7*$^{fl/fl}$ versus *Foxp3*^{Cre}*Atg7*$^{+/fl}$ T_{reg} cells, and rapamycin-treated *Foxp3*^{Cre}*Atg7*$^{fl/fl}$ versus *Foxp3*^{Cre}*Atg7*$^{+/fl}$ T_{reg} cells (**d**). Red color denotes upregulated genes in *Foxp3*^{Cre}*Atg7*$^{fl/fl}$ T_{reg} cells, and blue color denotes downregulated genes in *Foxp3*^{Cre}*Atg7*$^{fl/fl}$ T_{reg} cells (**d**). (**e**) Measurement of ECAR in T_{reg} cells (from *Foxp3*^{Cre}*Atg7*$^{+/fl}$ and *Foxp3*^{Cre}*Atg7*$^{fl/fl}$ mice) stimulated with anti-CD3 and anti-CD28 for 4 h in the presence of DMSO or JQ-1. (**f**) Flow cytometry analyzing YFP-Foxp3 expression in divided T_{reg} cells (from *Foxp3*^{Cre}*Atg7*$^{+/fl}$ and *Foxp3*^{Cre}*Atg7*$^{fl/fl}$ mice) that were activated *in vitro* with anti-CD3 and anti-CD28, and IL-2 for 96 h in the presence of DMSO or JQ-1. Numbers above graphs indicate MFI of YFP-Foxp3. NS, not significant ($P > 0.05$); * $P < 0.05$ and ** $P < 0.001$ (one-way ANOVA in **e**). Data are representative of four (**a,f**), three (**b,c**) or two (**e**) experiments, or from one (**d**) experiments (mean ± s.e.m in **e**).

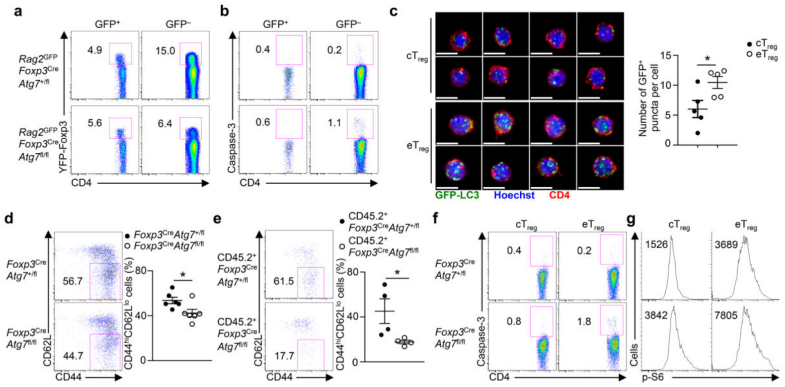

Figure 7. Autophagy is preferentially required for activated T_{reg} cell maintenance

(**a,b**) Flow cytometry analyzing the expression of YFP-Foxp3 in GFP$^+$ and GFP$^-$ CD4$^+$ T cells (**a**) and active caspase-3 in GFP$^+$ and GFP$^-$ T_{reg} cells (**b**) in the spleen of *Rag2*^{GFP}*Foxp3*^{Cre}*Atg7*$^{+/fl}$ and *Rag2*^{GFP}*Foxp3*^{Cre}*Atg7*$^{fl/fl}$ mice. Numbers adjacent to outlined areas indicate percent YFP-Foxp3$^+$ cells (**a**) and caspase-3$^+$ cells (**b**). (**c**) Representative images (scale bars, 5 μm) (left) and quantification of the number of GFP-LC3$^+$ puncta per cell (right) in cT_{reg} and eT_{reg} cells purified from the spleen of GFP-LC3 mice (n=5 mice). (**d,e**) Flow cytometry analyzing the proportion of CD44^{hi}CD62L^{lo} eT_{reg} cells among total T_{reg} cells in the spleen of *Foxp3*^{Cre}*Atg7*$^{+/fl}$ and *Foxp3*^{Cre}*Atg7*$^{fl/fl}$ mice (n=6 mice per genotype) (**d**, left) and *Foxp3*^{Cre}*Atg7*$^{+/fl}$ and *Foxp3*^{Cre}*Atg7*$^{fl/fl}$ chimeras (n=4 mice per group) (**e**, left), and frequency of CD44^{hi}CD62L^{lo} eT_{reg} cells (**d,e**, right). Numbers adjacent to outlined areas indicate percent CD44^{hi}CD62L^{lo} eT_{reg} cells (**d,e**, left). (**f,g**) Flow cytometry analyzing the expression of active caspase-3 (**f**) and p-S6 (**g**) in CD44^{lo}CD62L^{hi} cT_{reg} cells and CD44^{hi}CD62L^{lo} eT_{reg} cells in the spleen of *Foxp3*^{Cre}*Atg7*$^{+/fl}$ and *Foxp3*^{Cre}*Atg7*$^{fl/fl}$ mice. Numbers adjacent to outlined areas indicate percent caspase-3$^+$ cells (**f**), and numbers above graphs indicate MFI of p-S6 (**g**). * $P < 0.05$ (two-tail unpaired Student's *t*-test in **c–e**). Data are representative of five (**a,f**), three (**b,g**), or four (**e**) experiments, or pooled from two out of two (**c**) or five out of five (**d**) experiments (mean ± s.e.m in **c–e**).